

Cite as: M. Plass *et al.*, *Science*  
10.1126/science.aaq1723 (2018).

# Cell type atlas and lineage tree of a whole complex animal by single-cell transcriptomics

Mireya Plass,<sup>1\*</sup> Jordi Solana,<sup>1\*†</sup> F. Alexander Wolf,<sup>2</sup> Salah Ayoub,<sup>1</sup> Aristotelis Misios,<sup>1</sup> Petar Glažar,<sup>1</sup> Benedikt Obermayer,<sup>1‡</sup> Fabian J. Theis,<sup>2,3</sup> Christine Kocks,<sup>1</sup> Nikolaus Rajewsky<sup>1§</sup>

<sup>1</sup>Laboratory for Systems Biology of Gene Regulatory Elements, Berlin Institute for Medical Systems Biology, Max-Delbrück Center for Molecular Medicine, Germany.

<sup>2</sup>Helmholtz Zentrum München, German Research Center for Environmental Health, Institute of Computational Biology, Neuherberg, Germany. <sup>3</sup>Department of Mathematics, Technische Universität München, Germany.

\*These authors contributed equally to this work. †Present address: Department of Biological and Medical Sciences, Oxford Brookes University, Oxford, UK.

‡Present address: Core Unit Bioinformatics, Berlin Institute of Health, Berlin, Germany. §Corresponding author. Email: rajewsky@mdc-berlin.de

Flatworms of the species *Schmidtea mediterranea* are immortal—adult animals contain a large pool of pluripotent stem cells that continuously differentiate to all adult cell types. Therefore, single-cell transcriptome profiling of adult animals should reveal mature and progenitor cells. By combining perturbation experiments, gene expression analysis, a computational method that predicts future cell states from the transcriptional changes, and a lineage reconstruction method, we placed all major cell types onto a single lineage tree that connects all cells to a single stem cell compartment. We characterize gene expression changes during differentiation and discover cell types important for regeneration. Our results demonstrate the importance of single-cell transcriptome analysis for mapping and reconstructing fundamental processes of developmental and regenerative biology at high resolution.

Understanding differentiation from stem cells into the different cell types that make up the human body is a central problem of basic and medical science. Although numerous mechanisms of cellular differentiation have been identified and many cell types have been characterized, it will require a huge coordinated undertaking to systematically map all human cell types and cellular differentiation states (1). Due to the advances in single-cell transcriptomics, it has already been possible to study the cell type composition of mammalian organs and tissues (2–6) as well as development stages (7, 8). However, single-cell transcriptomics provide just a snapshot of the dynamics of the cell populations unless cells can be traced or tagged experimentally (9–12). Thus, reconstructing cell lineages from stem cells to differentiated cells remains a challenge. Recently, algorithms to order developmental states and compute lineage trees based on comparing single-cell transcriptomes have made considerable progress (13–15) and have revealed insights into stem cell biology (16) and tissue differentiation (17–20). However, these algorithms have been developed for the study of differentiation in specific cell lineages or tissues, and are not suitable to reconstruct all the cell differentiation trajectories present in complex animals.

Given these problems, can single-cell transcriptomic approaches improve our molecular understanding of how stem cells differentiate into all the cell types of an entire complex adult animal? Freshwater planarians such as *Schmidtea mediterranea* offer a unique opportunity to answer this question. Planarians are immortal, as they contain as adults

a large pool of pluripotent stem cells (neoblasts) that continuously differentiate to all mature cell types to turnover all tissues (21). Hence, all cell differentiation pathways are constantly active in adult individuals. We therefore reasoned that an unbiased single-cell transcriptomics approach should yield terminally differentiated cell types as well as a large number of intermediate cellular states, making planarians an ideal model system to attempt the lineage reconstruction of a whole animal.

Here we performed highly parallel droplet-based single-cell transcriptomics, Drop-seq (3), to characterize planarian cell types. We molecularly characterized dozens of cell types and uncovered many new ones. By applying a newly developed algorithm, PAGA, which reconciles the principles of clustering and pseudotemporal ordering (22), and combining it with independent computational and experimental approaches, we derive a consolidated lineage tree that includes all identified cell types rooted to a single stem cell cluster. Along this tree, we identify 48 gene sets that are co-regulated during the differentiation of specific cell types. Finally, we used single-cell transcriptomics to characterize the cellular processes that happen during regeneration. Our results reveal a strong depletion of newly characterized cell types, suggesting that these cells are used as an energy source for regeneration.

## A high-resolution cell type atlas for planaria

To comprehensively characterize different cell types and progenitor stages present in adult planarians, we performed

genome-wide expression profiling in individual cells using nanoliter droplets (Drop-seq) (3) of cells isolated from whole adult animals. These cells were obtained, after dissociation, by fluorescence-activated cell sorting (FACS), which separated intact live cells from dead cells and enucleated cellular debris (Fig. 1A). From 11 independent experiments, we captured a total of 21,612 cells. We detected on average 494 genes and ~970 transcripts (identified by using “unique molecular identifiers” (UMIs)) per cell. The individual datasets correspond to 5 wild type samples (10,866 cells), two RNAi samples (3314 cells), a high-DNA content G2/M population corresponding to cycling planarian stem cells (typically defined as X-ray sensitive “X1 cells”; 981 cells) (23, 24), and three wild type regeneration samples (6,451 cells; table S1). Sequencing depth was comparable across samples (fig. S1A). Biological replicates showed highly correlated gene expression profiles (fig. S1B). Besides, all samples showed high correlation with published RNA-seq data from equivalent bulk cell populations (24–27) (fig. S1C). We pooled and analyzed all single-cell datasets together using Seurat (3). 8 of 11 samples were fixed using methanol (28) or frozen with DMSO (29) to facilitate sample handling. To assess batch effects, we compared the overall quality across wild type samples. Cells from each batch were distributed similarly on the tSNE (fig. S1D), which resulted in comparable proportions of cells per cluster (fig. S1E, table S2). Although we observed a mild bias in gene expression due to the preservation procedure of the samples, clustering was not affected (fig. S1F). However, we observed differences in the number of UMIs per cell across clusters (fig. S1G). Together, these analyses confirmed that sample preparation did not compromise data quality or introduce bias. Therefore, we clustered the expression profiles of the individual cells from all samples together using Seurat (3). In total we identified 51 cell clusters (Fig. 1B).

We elucidated the cell type identity of clusters by examining marker genes and comparing them to previous literature (fig. S2A, B) (Supplementary Note 1). The largest cluster and 14 smaller clusters located in the center of the tSNE plot express combinations of well-known stem cell markers (fig. S3A), such as *Smedwi-1*, *Smedtud-1*, and *bruli* (fig. S3B). The remaining clusters corresponded to the previously described neural, epidermal, secretory, muscle, gut and protonephridia cell types (fig. S2A, S2B). However, in each of these categories, we found several distinct clusters (Fig. 1B) that express different combinations of marker genes (table S3, fig. S4). This result suggests that our approach can distinguish more cell types than previous studies.

### Single-cell transcriptomics unveils previously uncharacterized cell types

In the 1980's, Baguña and Romero used microscopy to mor-

phologically characterize and count all major cell types in *Schmidtea mediterranea* (30). We used this resource as a reference to validate cell types identified by our Drop-seq data and cluster annotation. Even though the microscopy data are of a qualitative nature, we observed a strong correlation between it and our molecular, unbiased Drop-seq annotation (Fig. 1C), suggesting that FACS sorting, cryopreservation or fixation and cell capture in nanodroplets did not influence cell type proportions. We validated the identity of several clusters by designing RNA probes targeting marker genes and performing in situ hybridizations, both whole mount and in histological sections (fig. S5). We could confirm major known cell types such as different types of neurons, muscle, protonephridia, epidermis, and secretory cells. We identified the two main cell types of the planarian gut: phagocytes (Fig. 1D, red) and goblet cells (Fig. 1D, green), and discovered markers of planarian goblet cells, including a gene without apparent homologs in other phyla. We named this gene *bruixot*. We also distinguished body and pharynx muscle (Fig. 1E). General muscle markers colocalized with body muscle markers in all the body except in the pharynx (Fig. 1E). Pharynx muscle was characterized by the expression of *laminin* (31) (fig. S5). The protonephridia cluster (0.3% of our wild type cells) contained the two main cell types of these organs, flame and tubular cells (32) (figs. S4, S5). In some cases, cell clusters contain several similar subtypes that we cannot distinguish at this resolution. For instance, previously described markers of eye pigment cup cells and photoreceptor neurons (33) are expressed in pigment and ChAT neurons 2 clusters respectively, indicating that the former are subtypes of the latter (fig. S6).

We also validated a recently discovered epidermis cell type, which marks the boundary between the dorsal and ventral parts of planarians (fig. S5) (34). Additionally, we identified an epidermal related pharynx cell type (fig. S5) and several parenchymal cell types previously undescribed molecularly (Fig. 2B, fig. S5). Among parenchymal clusters we found a diversity of non-overlapping cells types, including *aqp+* and the *psap+* parenchymal cells (Fig. 1F), which probably collectively correspond to the previously described fixed parenchymal cells (30, 35), pigment cells (cluster 44) (36, 37) and glial cells (38, 39) (cluster 47) (figs. S4, S5). Altogether these results show that we can identify known as well as unknown cell types using single-cell transcriptomics and measure their abundances in a reproducible way.

To investigate the function of newly identified cell types we used pathway and gene set overdispersion analysis (PAGODA) (40) to identify variable gene sets with particular gene ontology (GO) terms annotated (fig. S7, Supplementary Note 2). The clustering that emerges using these gene sets roughly recapitulates the one obtained with Seurat, showing

the robustness of our clustering approach (fig. S7A). This analysis revealed that neoblasts and progenitors are functionally similar, both expressing gene signatures enriched for GO terms related to RNA processing. Additionally, parenchymal clusters showed enrichment for GO terms related to *lysosome*, *extracellular region* and hydrolytic enzymes, and appear to share metabolic functions with gut cells (fig. S7B).

### Single-cell transcriptomics of purified stem cells and stem cell depleted animals reveals stem, progenitor and differentiated cell populations

The great diversity of cell types identified, which included stem cells, differentiated cells, and presumably many progenitor cells, offered a unique opportunity for exploring stem cell differentiation and lineage relationships between all cell clusters. We focused on the X1 cell sample, which is enriched in G2/M neoblasts (23, 24), and the *histone 2b* (*h2b*) RNAi treated whole planaria sample, in which stem and progenitor cell populations are depleted (41). Cells from these datasets showed a clear distribution pattern: X1 cells were located in the middle of the tSNE plot (Fig. 2A, red dots) whereas *h2b*(RNAi) resistant cells were clearly enriched in the periphery (Fig. 2A, blue dots). This distribution was specific and not the result of batch effects, as evident from the respective control samples (Fig. 2A, X1 control and *gfp*(RNAi) samples). Given that each dataset is enriched in particular cell populations, we reasoned that they could be used to distinguish cells in varying differentiation states. We quantified the fraction of cells per cluster from the X1 and *h2b*(RNAi) samples and compared them to wild type and control samples. We performed a principal component analysis (PCA) using these cellular proportions as well as the mean expression of the three top neoblast markers (*Smed-wi-1*, *tub- $\alpha$ 1* and *h2b*) in each cluster. The first two principal components resulting from this analysis separated clusters according to their gene expression profiles as neoblasts, progenitors, and differentiated cell clusters (Fig. 2B, fig. S2A). Mapping onto the tSNE revealed that progenitor cell clusters were located between differentiated cells and neoblast clusters (Fig. 2B). To corroborate the differentiation state of the cells in the different clusters, we pooled the cells in each group and correlated their gene expression profiles to previously described FACS populations. Neoblasts clusters best correlated with X1 populations, corresponding to high content DNA G2/M neoblasts, progenitor clusters correlated with X2 populations, a mixture of G1/S neoblasts and early progenitors, and differentiated cell clusters correlated with Xins samples, a pool of all differentiated cells (Fig. 2C). Altogether, our functional experiments reveal the stem, progenitor, or differentiated status of each cell cluster.

### Computational lineage reconstruction predicts a single tree for all major planarian cell differentiation trajectories

Existing methods to investigate cell differentiation using single-cell transcriptomics data were designed to study individual lineages or organs, allow few branching trajectories (13, 15, 18), and often require high sequencing depth and associated costs (16). To overcome these limitations, we developed the general framework of partition-based graph abstraction (PAGA), which reconciles clustering and pseudotemporal ordering algorithms and allows to infer complex cell trajectories and differentiation trees (22). Starting from the neighborhood-graph of single cells, in which cells are represented as nodes, the algorithm quantifies the connectivity of cell clusters and generates a much simpler abstracted graph in which nodes correspond to the clusters identified using Seurat and edges represent putative transitions between clusters. The differentiation tree is then computed as the tree-like subgraph in the abstracted graph that best explains all continuous progressions along the original single-cell graph (Supplementary Note 3).

When running this algorithm, without any assumptions about the tree structure, we obtained an abstracted graph that shows high confidence of the branching events (Fig. 3A) from which we can derive a single differentiation tree that included all the cell types and linked them to a single root, the neoblast 1 cluster. This tree defines independent differentiation branches for all the major tissues such as neurons, muscle, parenchyma, and gut (Fig. 3A). Additionally, the tree reflects the relation between different groups of cells. For example, it predicts the existence of independent progenitor cells for the epidermis dorso-ventral boundary and the pharynx cell type lineages although both lineages are related to the epidermal lineage. In contrast, it shows the presence of a shared progenitor for all parenchymal lineages despite containing cell types as different as glia and pigment cells. The connections in the tree are highly consistent with the continuity of gene expression patterns along the various lineages (fig. S8A) except for two cases: the epidermis cluster itself is disconnected from epidermal lineage, and muscle pharynx is connected to muscle body instead of muscle progenitors (fig. S8A). Together, from 51 clusters (with 1275 possible transitions between them), PAGA predicts 53 transitions that are mainly consistent with our marker based analysis.

Furthermore, PAGA yields a pseudotemporal ordering of individual cells within each cluster consistent with our stem cell ablation and purification experiments, and therefore confidently predicts their differentiation status, even for cell types for which separate progenitor clusters could not be identified (fig. S8B). For instance, when we sorted the goblet cells by pseudotime, we observe a higher percentage of X1

cells in early pseudotime and *h2b(RNAi)* cells in the late pseudotime (fig. S8B). To validate this observation, we performed double FISH of *bruixot*, our newly identified goblet cell marker, and *adb* (*aprenent de bruixot*), a gene expressed earlier in the goblet cluster pseudotime (fig. S8B). Consistently, *adb* was expressed in the gut (fig. S8C) overlapping with *bruixot*, but staining more cells located in the periphery of the gut that clearly lacked goblet cell morphology (fig. S8D). This indicates that *adb* is a marker of immature goblet cells and that computationally estimated pseudotime correctly orders cells according to their differentiation status.

Although the tree predicts the connectivity of cell clusters, it does not give any information about the direction of the trajectories. Thus, we used the tree topology to estimate the developmental potency of each cluster, i.e., their ability to give rise to other cells. We developed a potency score that is conceptually similar to the stemID score previously proposed to identify stem cells (16) but additionally estimates pluripotency vs. multi- or unipotency of cell populations. It is computed as the normalized degree of each cluster in the abstracted graph (Supplementary Note 4). This analysis showed that neoblast 1, the largest stem cell cluster, had a score of 1 (Fig. 3B), correctly assigning pluripotency to neoblasts as expected from earlier literature (21). We note that the potency score is independent of prior information and therefore can be used to identify stem cells from single-cell transcriptomics data alone, a feature that is particularly useful in less well-studied non-model organisms. Progenitor clusters showed lower potency than neoblasts, and higher potency scores than differentiated cells (Fig. 3B), in agreement with a gradual potency loss. To assess the stem cell and progenitor status of the clusters connected in the center of the PAGA topology, we mapped X1 and *h2b(RNAi)* data onto the tree. Most X1 cells were located in the neoblast 1 cluster (Fig. 3C) whereas *h2b(RNAi)* resistant cells were more enriched in the leaves of the tree (Fig. 3D). Thus, both PAGA and stem cell ablation and purification independently support the stem and progenitor status of these clusters.

The remaining neoblast clusters had lower potency scores than the neoblast cluster 1 and were connected to it. These clusters share the majority of marker genes with the neoblast 1 cluster (table S3) and do not correspond to previously identified specialized neoblasts of the sigma, gamma and zeta class (26, 42, 43) (fig. S9). Although some of these neoblast clusters are connected to differentiated cell types (Fig. 3A), most do not give rise to differentiated cell types, raising the possibility that they represent neoblasts in different metabolic, cell cycle or activation states (Supplementary Note 5).

We detect expression of specialized neoblast markers among both neoblast and progenitor clusters (figs. S10, S11).

Although present in neoblasts, sigma markers were most highly expressed in neural and muscle progenitors, gamma markers in gut, and parenchymal progenitors and zeta markers in epidermal progenitors (fig. S9D). These clusters are mostly devoid of X1 cells (Fig. 3C) and therefore correspond mainly to post-mitotic progenitors.

### RNA velocity confirms lineage relationships predicted by PAGA

To independently validate the differentiation trajectories predicted by PAGA we used velocity (44). This method computes RNA *velocity*, defined as the rate of change of mRNA levels for a gene in time, in every single cell. In differentiating cells in which changes in gene expression are dominated by changes in transcription rates, the ratio of unspliced to spliced reads for a given gene within a cell will be proportional to the temporal change of the logarithm of spliced reads (or mature mRNAs) (44). Thus, one can estimate the future mRNA level of a gene by computing its *velocity* and a linear fit. By aggregating over many genes in a cell, one can estimate the cellular expression state to which the cell is apparently moving in time. We estimated mRNA velocities for each cell and projected the estimated future states of cells onto the tSNE, which describe the paths predicted by the mRNA velocity model (Fig. 3E and fig. S12A). These paths show a highly homogenous stem cell population that moves slowly to progenitors, which will differentiate to mature cell types. The long arrows at the edges of the clusters likely are due to the averaging on the force field, as they do not appear when individual arrows are plotted (fig. S12A). These paths largely agree with the trajectories predicted by PAGA, and also confirmed the connection between muscle progenitors and pharynx muscle predicted from gene expression changes (fig. S12A). Additionally, velocity can also model longer cell trajectories in order to identify their root (Fig. 3F) and terminal end points (Fig. 3G), which corresponded to the tSNE regions containing stem cells and terminally differentiated cells, respectively. Velocity cannot provide information from disconnected clusters. As a result, all disconnected clusters contain differentiation trajectories with independent start and end points (Fig. 3F, G).

The estimates of RNA dynamics obtained with velocity also identified regions where genes are mainly induced or repressed compared to the steady state level. This information can be helpful to investigate relations between clusters that appear disconnected on the tSNE. We used these estimates to study the expression of marker genes from the epidermis cluster. These genes are clearly induced in epidermal progenitors and repressed in mature epidermis, where they are mainly expressed (fig. S12B). Thus, mRNA metabolism patterns provide additional support to the differentiation trajectory connecting late epidermal progeni-

tors to epidermis that we predicted based on gene expression changes (fig. S8A).

### **A consolidated lineage tree of planarian stem cell differentiation into all major cell types**

Taken together, our results show that both computational and experimental methods agree in the identification of stem cells, progenitors and differentiated cells. By combining all four independent lines of evidence (PAGA, gene expression changes, stem cell ablation and enrichment experiments, and velocity) we provide a single consolidated tree that models stem cell differentiation trajectories into all identified cell types of adult planarians (Fig. 4A). The resulting cell lineage tree correctly recapitulates the known expression changes described during epidermal differentiation (26, 34, 45) (Fig. 4B). We observed a continuous decrease of the expression of *Smedwi-1*, a well characterized neoblast marker (fig. S3), with pseudotime progression whereas early (*prog-1*) and late (*agat-1*) epidermal progenitor as well as mature epidermis (*vim-1*) markers increased their expression at consecutive time points (Fig. 4B).

According to the consolidated lineage tree, neoblasts (35% of our wild type cells) differentiate into at least 23 independent cell lineages. There are 6 major differentiation fates (57% of cells) (table S2), each representing more than 1% of total cells: epidermal, parenchymal, neural, muscle, gut, and a pharynx cell type. For these major fates, we identified progenitor and differentiated states. Additionally, we identified 10 minor lineages (6% cells; each less abundant than 1% of total cells) that differentiate from the neoblasts, but for which we were unable to identify progenitors.

### **Self-organizing maps identify gene programs underlying cell differentiation**

We used our data to identify gene sets that coordinately change their expression during differentiation. For this analysis, we discarded all cells from neoblast clusters that did not give rise to differentiated cell types in our consolidated cell lineage tree. The remaining cells were ordered following the tree for each lineage and sorted within each cluster according to their pseudotemporal ordering (Fig. 5A). Subsequently, we used self-organizing maps (SOMs) (46) to identify 48 sets of highly variable genes that coordinately change their expression during differentiation (47) (Fig. 5B, fig. S13 and table S4). Many of these sets contain some genes previously known to be expressed in the respective lineages and in some cases involved in their differentiation (table S5). For instance, gene sets 10 and 11 contain genes that are highly expressed in neoblast and progenitor clusters, such as *Smedwi-1* and *tub- $\alpha$ -1*, whose expression drops during differentiation (Fig. 5B and fig. S13). Similarly, we found gene sets that are regulated along muscle, neu-

ronal, parenchymal, gut and epidermal differentiation (Fig. 5B, top row). They contained genes expressed in these lineages, such as *mhc* for the muscle and *chat* for the neuronal lineage, but also included well-known regulators of their differentiation, such as *myoD* (48) and *coe* (49). As a consequence of analyzing all detected planarian cell lineages simultaneously, we not only identified gene sets involved in lineage specific programs but also gene sets co-regulated during the differentiation of several fates (Fig. 5B, mid and bottom row). Taken together, these results show that single-cell transcriptomics of a whole organism allows the reconstruction of specific differentiation events for many differentiation fates in parallel, enabling the identification of previously undetected combinations of co-regulated genes.

### **Molecular profiling of planarian regeneration by single-cell transcriptomics**

Freshwater planarians are well known for their remarkable regenerative capacities. Planarians can be cut into small pieces, and each piece (except for the pharynx and the most anterior tip of the head which are devoid of neoblasts) can regenerate a complete, albeit much smaller, organism in a matter of days. This process is dynamically complex and involves the orchestration of all cellular differentiation pathways. The animal does not grow (as it cannot eat) during the process. Thus, the truncated body fragments need to reshape their body proportions to adjust to their new size by the process termed morphallaxis (50). It is still largely unknown how each individual cell type behaves in this process.

Given the detected cell type abundances and the cell differentiation tree of steady state adult animals, we asked if we could use Drop-Seq to profile the cellular and transcriptomic changes that occur during regeneration. We cut planarians in 5-7 pieces, discarded the head piece and prepared the remaining body pieces for single-cell transcriptomics immediately after cutting (day 0), and 2 and 4 days after cut (Fig. 6A, fig. S14). We compared regenerating samples to day 0 using Seurat and detected hundreds of differentially expressed genes in both samples (tables S6, S7). By pooling all cells we were able to detect upregulation after 2 days of regeneration of 16 of the 128 wound induced genes described in a previous study (42, 51) (table S6, fig. S15A). The shallowness of Drop-seq data makes difficult to assess differences in lowly expressed genes. However, Drop-seq allows distinguishing the cell types that undergo these changes, showing that *runt-1* and *egr-2* are upregulated in the neoblast 1 cluster (fig. S15B) and *jun-1* in the muscle body cluster (fig. S15C; tables S7, S8).

All cells from the regenerating samples fall into clusters that are present in wild type samples, indicating an absence of regeneration-specific types or trajectories (table S2).

However our analysis revealed significant changes in cell composition during regeneration: on one hand, we observed a large increase in the number of neoblasts, consistent with an increase in mitotic activity, and of neural progenitors, reflecting active neurogenesis to replace missing brain structures after head removal (Fig. 6B, fig. S16). On the other hand, we detected that both parenchymal progenitor cells and differentiated parenchymal cell types were depleted (Fig. 6B, fig. S16), indicating that these cells are cleared in the process of reshaping the planarian tissue. The cell proportion changes at day 2 and 4 were clearly correlated (Fig. 6C), indicating that *aqp*<sup>+</sup> parenchymal cells are the most depleted cell type. We experimentally confirmed this observation by in situ hybridization on planarian tissue sections (Fig. 6D) and counting *aqp*<sup>+</sup> parenchymal cells (Fig. 6E) (Mann Whitney U-test p-value < 1e-7). Our results indicate that parenchymal cells are highly depleted upon regeneration, implying that they may be used to metabolically fuel the regeneration process (52).

## Discussion

In this study, we used the stem cell population and the extreme regeneration capabilities of adult flatworms to generate an atlas of cell types at high resolution. We identified, quantified, and molecularly characterized 37 cell types including 23 terminally differentiated cell types, and numerous progenitor and stem cells clusters. Although our sequencing data are relatively shallow, molecular characterization of cell types using computational methods was robust, agreed well with previously published microscopy data, and revealed progenitor and differentiated cells. This implies that the grouping of incomplete transcriptomes of thousands of cells into clusters did not suffer significantly from capture rates or other confounding factors.

The resolution of our data depends on both the number of cells sequenced and the number of genes detected per cell. Considering only wt and control samples (~11,000 cells), we can identify differentiated cell clusters containing about 10 cells. Therefore, we estimate that cells present at a frequency of <1:1000, such as *cintillo*<sup>+</sup> cells (53) and photoreceptor neurons (33), will be missed by our approach. Besides, we failed to identify certain neoblast subpopulations previously described in the literature (26, 42). This result could be due to the low sensitivity of Drop-seq, which captures only a fraction of mRNAs in a cell. However, we do detect the expression of the proposed marker genes of these subpopulations. They appear to be spread among neoblasts and progenitor clusters (fig. S8), which still express neoblast markers such as *Smedwi-1* at low levels (figs. S3, S11). This indicates that the boundary between stem cells and lineage-committed progenitors is probably not sharp. Further studies will help describing and delimiting these boundaries.

Projecting high dimensional gene expression data of thousands of transcriptomes onto a two-dimensional plot (for example by the widely used tSNE method (54)) visually reveals clusters. However, it is impossible to infer the relationships among them, as the distances between clusters cannot be interpreted as differentiation trajectories. To solve this problem, we used computational and experimental methods to reconstruct a lineage tree. PAGA and velocity provide two complementary approaches to study cell differentiation using single-cell transcriptomics. While velocity allows finding the differentiation trajectories of individual cells within a cell continuum based on RNA metabolism, PAGA allows inferring the average differentiation paths of a group of cells, even when they are disconnected. Thus, combining these two computational methods results in a robust lineage prediction. This prediction is supported by the continuity of expression of marker genes and the mapping of stem cells and differentiated cells on the tree (Fig. 4A), and validates known differentiation trajectories such as that of the epidermal lineage (Fig. 4B) (34).

We used PAGA (22) to reconstruct in an unbiased way the lineage tree of all major planarian cells. This method, although indirect, allows reconstructing the lineage information from the transcriptomic snapshot of individual cells. Besides, in contrast to high throughput lineage tracing methods (9–12), which rely on using transgenic or CRISPR/Cas tools, it can be applied to every species provided that single cells can be isolated and sequenced. Using this method, we identified de novo planarian stem cells and predict their differentiation paths to at least 23 different lineages, including several multipotent progenitor populations. Importantly, these tools can readily be applied to other organism to identify de novo stem cells, identify their differentiation trajectories and estimate the developmental potency of the resulting cell populations.

Pseudotemporal ordering of cells along these lineages allowed us to discover gene sets that are putatively involved in differentiation programs, highlighting the similarities and differences that exist across tissues, and identifying several genes known to be involved in cell differentiation not only in planarians but also in other species, such as *myoD*, *nkx6* and *pax6*. Further characterization of these gene sets should be the subject of future studies. As we show for the *h2b* RNAi phenotype, Drop-seq also allows profiling perturbation studies at both the transcriptomic and cellular levels. In general, and beyond planaria, we can foresee that future studies will use single-cell transcriptomics coupled to loss-of-function experiments to unravel the specific developmental functions of genes or regulatory networks.

Furthermore, we used single-cell transcriptomics to profile cellular abundance changes upon regeneration. Our experiments revealed that several of our newly described

parenchymal types are depleted in regeneration. These cell types had been largely overlooked in molecular studies but had been described, based on microscopy, in the literature decades ago. This is in part due to the unbiased nature of both microscopic and single-cell transcriptomic data. We note that these parenchymal cells are highly enriched in lysosomes and other vacuoles and might be an energy reservoir that regenerating planarians mobilize to fuel regeneration.

To make our data easily accessible, we built an interactive app that allows to query and interpret all sequencing data (<https://shiny.mdc-berlin.de/psca>). We also provide a detailed tutorial for the lineage reconstruction algorithm PAGA that we hope will serve as a reference for future studies ([https://github.com/rajewsky-lab/planarian\\_lineages](https://github.com/rajewsky-lab/planarian_lineages)). Together, our results show that single-cell expression profiling can be used to systematically annotate cell types of entire animals, to reconstruct stem cell differentiation lineages of whole organisms, and to study complex processes such as regeneration (and their relation to lineages used in normal development) at single-cell resolution. Our results and methods demonstrate that single-cell approaches will become an indispensable method to study developmental and regeneration biology.

### Methods summary

Single-cell transcriptomic profiling of asexual adult planarians from the species *Schmidtea mediterranea* was performed using Drop-seq. Single cell suspensions were prepared by dissociating cells from adult planarians of 4-10 mm in length using trypsin. We used FACS to discard broken and dead cells. Cells were either directly processed for Drop-seq or preserved in methanol or DMSO for later processing. For RNAi experiments, animals were injected with dsRNA against the coding region of *h2b* or *gfp* for three consecutive days, kept at 20°C, and their cells prepared for FACS and single cell transcriptomics 5 days after the third injection. For regeneration experiments, animals ranging 4-10 mm in size were cut in 5-7 pieces, the head pieces were discarded and the remaining pieces were processed for Drop-seq immediately, 2 or 4 days after cut.

Computational analysis of the sequenced samples was done using Dropseq tools and the Seurat package (3). Briefly, reads were mapped to the *S. mediterranea* dd\_Smed\_v6 transcriptome and processed using Dropseq tools and custom perl scripts to generate Digital Gene Expression (DGE) matrices for each sample. Finally, all DGE matrices were joined. Variable genes across all clusters were used to perform a Principal Component Analysis (PCA). The first 50 PCs obtained were then tested for significance and those with a p-value < 10e-5 were used to perform clustering. The robustness of the obtained clusters was assessed and spuri-

ous clusters were merged to obtain a final set of 51 clusters.

Cell type identification was performed by calculating marker genes for each cluster. Manual inspection, comparison to previously published single-cell data, and experimental validation using in situ hybridizations of the marker genes reported allowed the identification of the different cell populations. Additional characterization of the identified cell types was performed by characterizing GO-term based gene sets using PAGODA (40). Experimental validation of cell types was done using whole mount in situ hybridization and in situ hybridization on histological sections as previously described and using probes complementary to marker genes (table S9).

Lineage reconstruction was done by combining the unsupervised graph obtained with the PAGA algorithm (22) with velocity (44), gene expression analysis, and experimental data from *h2b(RNAi)* and X1 facs sorted cells. To calculate RNA velocity with velocity, we mapped the reads from all datasets to the planarian genome in order to extract spliced and unspliced reads. These analyses allowed us to obtain a pseudotemporal order of cells that was used to identify gene sets that change during stem cell differentiation using self-organizing maps.

To preform cell counting of regenerating planarians, positive cells were automatically counted using a custom script for ImageJ (<https://imagej.net>).

### REFERENCES AND NOTES

1. A. Regev, S. A. Teichmann, E. S. Lander, I. Amit, C. Benoist, E. Birney, B. Bodenmiller, P. Campbell, P. Carninci, M. Clatworthy, H. Clevers, B. Deplancke, I. Dunham, J. Eberwine, R. Eils, W. Enard, A. Farmer, L. Fugger, B. Göttgens, N. Hacohen, M. Haniffa, M. Hemberg, S. Kim, P. Klenerman, A. Kriegstein, E. Lein, S. Linnarsson, E. Lundberg, J. Lundeberg, P. Majumder, J. C. Marioni, M. Merad, M. Mhlanga, M. Nawijn, M. Netea, G. Nolan, D. Pe'er, A. Philippakis, C. P. Ponting, S. Quake, W. Reik, O. Rozenblatt-Rosen, J. Sanes, R. Satija, T. N. Schumacher, A. Shalek, E. Shapiro, P. Sharma, J. W. Shin, O. Stegle, M. Stratton, M. J. T. Stubbington, F. J. Theis, M. Uhlen, A. van Oudenaarden, A. Wagner, F. Watt, J. Weissman, B. Wold, R. Xavier, N. Yosef; Human Cell Atlas Meeting Participants, The Human Cell Atlas. *eLife* **6**, e27041 (2017). doi:10.7554/eLife.27041 Medline
2. D. A. Jaitin, E. Kenigsberg, H. Keren-Shaul, N. Elefant, F. Paul, I. Zaretsky, A. Mildner, N. Cohen, S. Jung, A. Tanay, I. Amit, Massively parallel single-cell RNA-seq for marker-free decomposition of tissues into cell types. *Science* **343**, 776–779 (2014). doi:10.1126/science.1247651 Medline
3. E. Z. Macosko, A. Basu, R. Satija, J. Nemes, K. Shekhar, M. Goldman, I. Tirosh, A. R. Bialas, N. Kamitaki, E. M. Martersteck, J. J. Trombetta, D. A. Weitz, J. R. Sanes, A. K. Shalek, A. Regev, S. A. McCarroll, Highly parallel genome-wide expression profiling of individual cells using nanoliter droplets. *Cell* **161**, 1202–1214 (2015). doi:10.1016/j.cell.2015.05.002 Medline
4. K. Shekhar, S. W. Lapan, I. E. Whitney, N. M. Tran, E. Z. Macosko, M. Kowalczyk, X. Adiconis, J. Z. Levin, J. Nemes, M. Goldman, S. A. McCarroll, C. L. Cepko, A. Regev, J. R. Sanes, Comprehensive classification of retinal bipolar neurons by single-cell transcriptomics. *Cell* **166**, 1308–1323.e30 (2016). doi:10.1016/j.cell.2016.07.054 Medline
5. A. C. Villani, R. Satija, G. Reynolds, S. Sarkizova, K. Shekhar, J. Fletcher, M. Griesbeck, A. Butler, S. Zheng, S. Lazo, L. Jardine, D. Dixon, E. Stephenson, E. Nilsson, I. Grundberg, D. McDonald, A. Filby, W. Li, P. L. De Jager, O. Rozenblatt-Rosen, A. A. Lane, M. Haniffa, A. Regev, N. Hacohen, Single-cell RNA-seq reveals new types of human blood dendritic cells, monocytes, and progenitors. *Science* **356**, eaah4573 (2017). doi:10.1126/science.aah4573 Medline

6. D. Grün, A. Lyubimova, L. Kester, K. Wiebrands, O. Basak, N. Sasaki, H. Clevers, A. van Oudenaarden, Single-cell messenger RNA sequencing reveals rare intestinal cell types. *Nature* **525**, 251–255 (2015). [doi:10.1038/nature14966](https://doi.org/10.1038/nature14966) [Medline](#)
7. N. Karaïskos, P. Wahle, J. Alles, A. Boltengagen, S. Ayoub, C. Kipar, C. Kocks, N. Rajewsky, R. P. Zinzen, The *Drosophila* embryo at single-cell transcriptome resolution. *Science* **358**, 194–199 (2017). [doi:10.1126/science.aan3235](https://doi.org/10.1126/science.aan3235) [Medline](#)
8. J. Cao, J. S. Packer, V. Ramani, D. A. Cusanovich, C. Huynh, R. Daza, X. Qiu, C. Lee, S. N. Furlan, F. J. Steemers, A. Adey, R. H. Waterston, C. Trapnell, J. Shendure, Comprehensive single-cell transcriptional profiling of a multicellular organism. *Science* **357**, 661–667 (2017). [doi:10.1126/science.aam8940](https://doi.org/10.1126/science.aam8940) [Medline](#)
9. A. McKenna, G. M. Findlay, J. A. Gagnon, M. S. Horwitz, A. F. Schier, J. Shendure, Whole-organism lineage tracing by combinatorial and cumulative genome editing. *Science* **353**, aaf7907 (2016). [doi:10.1126/science.aaf7907](https://doi.org/10.1126/science.aaf7907) [Medline](#)
10. K. L. Frieda, J. M. Linton, S. Hormoz, J. Choi, K. K. Chow, Z. S. Singer, M. W. Budde, M. B. Elowitz, L. Cai, Synthetic recording and in situ readout of lineage information in single cells. *Nature* **541**, 107–111 (2017). [doi:10.1038/nature20777](https://doi.org/10.1038/nature20777) [Medline](#)
11. B. Spanjaard *et al.*, Simultaneous lineage tracing and cell-type identification using CRISPR–Cas9-induced genetic scars. *Nat. Biotechnol.* **2018**, 24 (2018). [10.1038/nbt.4124](https://doi.org/10.1038/nbt.4124)
12. A. Alemany, M. Florescu, C. S. Baron, J. Peterson-Maduro, A. van Oudenaarden, Whole-organism clone tracing using single-cell sequencing. *Nature* **556**, 108–112 (2018). [doi:10.1038/nature25969](https://doi.org/10.1038/nature25969) [Medline](#)
13. L. Haghverdi, M. Büttner, F. A. Wolf, F. Büttner, F. J. Theis, Diffusion pseudotime robustly reconstructs lineage branching. *Nat. Methods* **13**, 845–848 (2016). [doi:10.1038/nmeth.3971](https://doi.org/10.1038/nmeth.3971) [Medline](#)
14. M. Setty, M. D. Tadmor, S. Reich-Zeliger, O. Angel, T. M. Salame, P. Kathail, K. Choi, S. Bendall, N. Friedman, D. Pe'er, Wishbone identifies bifurcating developmental trajectories from single-cell data. *Nat. Biotechnol.* **34**, 637–645 (2016). [doi:10.1038/nbt.3569](https://doi.org/10.1038/nbt.3569) [Medline](#)
15. X. Qiu, Q. Mao, Y. Tang, L. Wang, R. Chawla, H. A. Pliner, C. Trapnell, Reversed graph embedding resolves complex single-cell trajectories. *Nat. Methods* **14**, 979–982 (2017). [doi:10.1038/nmeth.4402](https://doi.org/10.1038/nmeth.4402) [Medline](#)
16. D. Grün, M. J. Muraro, J.-C. Boisset, K. Wiebrands, A. Lyubimova, G. Dharmadhikari, M. van den Born, J. van Es, E. Jansen, H. Clevers, E. J. P. de Koning, A. van Oudenaarden, De novo prediction of stem cell identity using single-cell transcriptome data. *Cell Stem Cell* **19**, 266–277 (2016). [doi:10.1016/j.stem.2016.05.010](https://doi.org/10.1016/j.stem.2016.05.010) [Medline](#)
17. F. Notta, S. Zandi, N. Takayama, S. Dobson, O. I. Gan, G. Wilson, K. B. Kaufmann, J. McLeod, E. Laurenti, C. F. Dunant, J. D. McPherson, L. D. Stein, Y. Dror, J. E. Dick, Distinct routes of lineage development reshape the human blood hierarchy across ontogeny. *Science* **351**, aab2116 (2016). [doi:10.1126/science.aab2116](https://doi.org/10.1126/science.aab2116) [Medline](#)
18. J. Shin, D. A. Berg, Y. Zhu, J. Y. Shin, J. Song, M. A. Bonaguidi, G. Enikolopov, D. W. Nauen, K. M. Christian, G. L. Ming, H. Song, Single-cell RNA-Seq with Waterfall reveals molecular cascades underlying adult neurogenesis. *Cell Stem Cell* **17**, 360–372 (2015). [doi:10.1016/j.stem.2015.07.013](https://doi.org/10.1016/j.stem.2015.07.013) [Medline](#)
19. B. Treutlein, D. G. Brownfield, A. R. Wu, N. F. Neff, G. L. Mantalas, F. H. Espinoza, T. J. Desai, M. A. Krasnow, S. R. Quake, Reconstructing lineage hierarchies of the distal lung epithelium using single-cell RNA-seq. *Nature* **509**, 371–375 (2014). [doi:10.1038/nature13173](https://doi.org/10.1038/nature13173) [Medline](#)
20. L. Velten, S. F. Haas, S. Raffel, S. Blaszkiewicz, S. Islam, B. P. Hennig, C. Hirche, C. Lutz, E. C. Buss, D. Nowak, T. Boch, W.-K. Hofmann, A. D. Ho, W. Huber, A. Trumpp, M. A. G. Essers, L. M. Steinmetz, Human haematopoietic stem cell lineage commitment is a continuous process. *Nat. Cell Biol.* **19**, 271–281 (2017). [doi:10.1038/ncb3493](https://doi.org/10.1038/ncb3493) [Medline](#)
21. D. E. Wagner, I. E. Wang, P. W. Reddien, Clonogenic neoblasts are pluripotent adult stem cells that underlie planarian regeneration. *Science* **332**, 811–816 (2011). [doi:10.1126/science.1203983](https://doi.org/10.1126/science.1203983) [Medline](#)
22. F. A. Wolf, F. Hamey, M. Plass, J. Solana, J. S. Dahlin, B. Gottgens, N. Rajewsky, L. Simon, F. J. Theis, Graph abstraction reconciles clustering with trajectory inference through a topology preserving map of single cells. [bioRxiv 208819](https://doi.org/10.1101/208819) [Preprint]. 25 October 2017.
23. T. Hayashi, M. Asami, S. Higuchi, N. Shibata, K. Agata, Isolation of planarian X-ray-sensitive stem cells by fluorescence-activated cell sorting. *Dev. Growth Differ.* **48**, 371–380 (2006). [doi:10.1111/j.1440-169X.2006.00876.x](https://doi.org/10.1111/j.1440-169X.2006.00876.x) [Medline](#)
24. P. Önal, D. Grün, C. Adamidi, A. Rybak, J. Solana, G. Mastrobuoni, Y. Wang, H.-P. Rahn, W. Chen, S. Kempa, U. Zibold, N. Rajewsky, Gene expression of pluripotency determinants is conserved between mammalian and planarian stem cells. *EMBO J.* **31**, 2755–2769 (2012). [doi:10.1038/emboj.2012.110](https://doi.org/10.1038/emboj.2012.110) [Medline](#)
25. R. M. Labbé, M. Irimia, K. W. Currie, A. Lin, S. J. Zhu, D. D. R. Brown, E. J. Ross, V. Voisin, G. D. Bader, B. J. Blencowe, B. J. Pearson, A comparative transcriptomic analysis reveals conserved features of stem cell pluripotency in planarians and mammals. *Stem Cells* **30**, 1734–1745 (2012). [doi:10.1002/stem.1144](https://doi.org/10.1002/stem.1144) [Medline](#)
26. J. C. van Wolfswinkel, D. E. Wagner, P. W. Reddien, Single-cell analysis reveals functionally distinct classes within the planarian stem cell compartment. *Cell Stem Cell* **15**, 326–339 (2014). [doi:10.1016/j.stem.2014.06.007](https://doi.org/10.1016/j.stem.2014.06.007) [Medline](#)
27. J. Solana, M. Irimia, S. Ayoub, M. R. Orejuela, V. Zywitzka, M. Jens, J. Tapial, D. Ray, Q. Morris, T. R. Hughes, B. J. Blencowe, N. Rajewsky, Conserved functional antagonism of CELF and MBNL proteins controls stem cell-specific alternative splicing in planarians. *eLife* **5**, e16797 (2016). [doi:10.7554/eLife.16797](https://doi.org/10.7554/eLife.16797) [Medline](#)
28. J. Alles, N. Karaïskos, S. D. Praktijnjo, S. Grosswendt, P. Wahle, P.-L. Ruffault, S. Ayoub, L. Schreyer, A. Boltengagen, C. Birchmeier, R. Zinzen, C. Kocks, N. Rajewsky, Cell fixation and preservation for droplet-based single-cell transcriptomics. *BMC Biol.* **15**, 44 (2017). [doi:10.1186/s12915-017-0383-5](https://doi.org/10.1186/s12915-017-0383-5) [Medline](#)
29. A. Guillaumet-Adkins, G. Rodríguez-Esteban, E. Mereu, M. Mendez-Lago, D. A. Jaitin, A. Villanueva, A. Vidal, A. Martínez-Martí, E. Felip, A. Vivancos, H. Keren-Shaul, S. Heath, M. Gut, I. Amit, I. Gut, H. Heyn, Single-cell transcriptome conservation in cryopreserved cells and tissues. *Genome Biol.* **18**, 45 (2017). [doi:10.1186/s13059-017-1171-9](https://doi.org/10.1186/s13059-017-1171-9) [Medline](#)
30. J. Baguña, R. Romero, Quantitative-analysis of cell-types during growth, Degrowth and Regeneration in the Planarians *Dugesia-Mediterranea* and *Dugesia-Tigrina*. *Hydrobiologia* **84**, 181–194 (1981). [doi:10.1007/BF00026179](https://doi.org/10.1007/BF00026179)
31. F. Cebrià, P. A. Newmark, Morphogenesis defects are associated with abnormal nervous system regeneration following roboA RNAi in planarians. *Development* **134**, 833–837 (2007). [doi:10.1242/dev.02794](https://doi.org/10.1242/dev.02794) [Medline](#)
32. J. C. Rink, H. T.-K. Vu, A. Sánchez Alvarado, The maintenance and regeneration of the planarian excretory system are regulated by EGFR signaling. *Development* **138**, 3769–3780 (2011). [doi:10.1242/dev.066852](https://doi.org/10.1242/dev.066852) [Medline](#)
33. S. W. Lapan, P. W. Reddien, Transcriptome analysis of the planarian eye identifies ovo as a specific regulator of eye regeneration. *Cell Reports* **2**, 294–307 (2012). [doi:10.1016/j.celrep.2012.06.018](https://doi.org/10.1016/j.celrep.2012.06.018) [Medline](#)
34. O. Wurtzel, I. M. Oderberg, P. W. Reddien, Planarian epidermal stem cells respond to positional cues to promote cell-type diversity. *Dev. Cell* **40**, 491–504.e5 (2017). [doi:10.1016/j.devcel.2017.02.008](https://doi.org/10.1016/j.devcel.2017.02.008) [Medline](#)
35. K. J. Pedersen, Studies on the nature of planarian connective tissue. *Z. Zellf. Mikrosk. Anat.* **53**, 569–608 (1961). [doi:10.1007/BF00339508](https://doi.org/10.1007/BF00339508)
36. B. M. Stubenhaus, J. P. Dustin, E. R. Neverett, M. S. Beaudry, L. E. Nadeau, E. Burk-McCoy, X. He, B. J. Pearson, J. Pelletier, Light-induced depigmentation in planarians models the pathophysiology of acute porphyrias. *eLife* **5**, e14175 (2016). [doi:10.7554/eLife.14175](https://doi.org/10.7554/eLife.14175) [Medline](#)
37. C. Wang, X.-S. Han, F.-F. Li, S. Huang, Y.-W. Qin, X.-X. Zhao, Q. Jing, Forkhead containing transcription factor Albino controls tetrapyrrole-based body pigmentation in planarian. *Cell Discov.* **2**, 16029 (2016). [doi:10.1038/celldisc.2016.29](https://doi.org/10.1038/celldisc.2016.29) [Medline](#)
38. I. E. Wang, S. W. Lapan, M. L. Scimone, T. R. Clandinin, P. W. Reddien, Hedgehog signaling regulates gene expression in planarian glia. *eLife* **5**, e16996 (2016). [doi:10.7554/eLife.16996](https://doi.org/10.7554/eLife.16996) [Medline](#)
39. R. H. Roberts-Galbraith, J. L. Brubacher, P. A. Newmark, A functional genomics screen in planarians reveals regulators of whole-brain regeneration. *eLife* **5**, e17002 (2016). [doi:10.7554/eLife.17002](https://doi.org/10.7554/eLife.17002) [Medline](#)
40. J. Fan, N. Salathia, R. Liu, G. E. Kaeser, Y. C. Yung, J. L. Herman, F. Kaper, J.-B. Fan, K. Zhang, J. Chun, P. V. Kharchenko, Characterizing transcriptional heterogeneity through pathway and gene set overdispersion analysis. *Nat. Methods* **13**, 241–244 (2016). [doi:10.1038/nmeth.3734](https://doi.org/10.1038/nmeth.3734) [Medline](#)
41. J. Solana, D. Kao, Y. Mihaylova, F. Jaber-Hijazi, S. Malla, R. Wilson, A. Aboobaker, Defining the molecular profile of planarian pluripotent stem cells using a combinatorial RNAseq, RNA interference and irradiation approach. *Genome Biol.* **13**, R19 (2012). [doi:10.1186/gb-2012-13-3-r19](https://doi.org/10.1186/gb-2012-13-3-r19) [Medline](#)

42. O. Wurtzel, L. E. Cote, A. Poirier, R. Satija, A. Regev, P. W. Reddien, A generic and cell-type-specific wound response precedes regeneration in planarians. *Dev. Cell* **35**, 632–645 (2015). [doi:10.1016/j.devcel.2015.11.004](https://doi.org/10.1016/j.devcel.2015.11.004) [Medline](#)
43. A. M. Molinaro, B. J. Pearson, In silico lineage tracing through single cell transcriptomics identifies a neural stem cell population in planarians. *Genome Biol.* **17**, 87 (2016). [doi:10.1186/s13059-016-0937-9](https://doi.org/10.1186/s13059-016-0937-9) [Medline](#)
44. G. La Manno *et al.*, RNA velocity in single cells. [bioRxiv](https://doi.org/10.1101/199961) 206052 [Preprint]. 19 October 2017.
45. G. T. Eisenhoffer, H. Kang, A. Sánchez Alvarado, Molecular analysis of stem cells and their descendants during cell turnover and regeneration in the planarian *Schmidtea mediterranea*. *Cell Stem Cell* **3**, 327–339 (2008). [doi:10.1016/j.stem.2008.07.002](https://doi.org/10.1016/j.stem.2008.07.002) [Medline](#)
46. T. Kohonen, The self-organizing map. *Proc. IEEE* **78**, 1464–1480 (1990). [doi:10.1109/5.58325](https://doi.org/10.1109/5.58325)
47. P. Tamayo, D. Slonim, J. Mesirov, Q. Zhu, S. Kitareewan, E. Dmitrovsky, E. S. Lander, T. R. Golub, Interpreting patterns of gene expression with self-organizing maps: Methods and application to hematopoietic differentiation. *Proc. Natl. Acad. Sci. U.S.A.* **96**, 2907–2912 (1999). [doi:10.1073/pnas.96.6.2907](https://doi.org/10.1073/pnas.96.6.2907) [Medline](#)
48. M. L. Scimone, L. E. Cote, P. W. Reddien, Orthogonal muscle fibres have different instructive roles in planarian regeneration. *Nature* **551**, 623–628 (2017). [doi:10.1038/nature24660](https://doi.org/10.1038/nature24660) [Medline](#)
49. M. W. Cowles, K. C. Omuro, B. N. Stanley, C. G. Quintanilla, R. M. Zayas, COE loss-of-function analysis reveals a genetic program underlying maintenance and regeneration of the nervous system in planarians. *PLOS Genet.* **10**, e1004746 (2014). [doi:10.1371/journal.pgen.1004746](https://doi.org/10.1371/journal.pgen.1004746) [Medline](#)
50. K. Agata, Y. Saito, E. Nakajima, Unifying principles of regeneration I: Epimorphosis versus morphallaxis. *Dev. Growth Differ.* **49**, 73–78 (2007). [doi:10.1111/j.1440-169X.2007.00919.x](https://doi.org/10.1111/j.1440-169X.2007.00919.x) [Medline](#)
51. D. Wenemoser, P. W. Reddien, Planarian regeneration involves distinct stem cell responses to wounds and tissue absence. *Dev. Biol.* **344**, 979–991 (2010). [doi:10.1016/j.ydbio.2010.06.017](https://doi.org/10.1016/j.ydbio.2010.06.017) [Medline](#)
52. C. González-Estévez, D. A. Felix, A. A. Aboobaker, E. Saló, Gtdap-1 promotes autophagy and is required for planarian remodeling during regeneration and starvation. *Proc. Natl. Acad. Sci. U.S.A.* **104**, 13373–13378 (2007). [doi:10.1073/pnas.0703588104](https://doi.org/10.1073/pnas.0703588104) [Medline](#)
53. N. J. Oviedo, P. A. Newmark, A. Sánchez Alvarado, Allometric scaling and proportion regulation in the freshwater planarian *Schmidtea mediterranea*. *Dev. Dyn.* **226**, 326–333 (2003). [doi:10.1002/dvdy.10228](https://doi.org/10.1002/dvdy.10228) [Medline](#)
54. L. Van Der Maaten, G. Hinton, Visualizing Data using t-SNE. *J. Mach. Learn. Res.* **9**, 2579–2605 (2008).
55. J. Solana, C. Gamberi, Y. Mihaylova, S. Grosswendt, C. Chen, P. Lasko, N. Rajewsky, A. A. Aboobaker, The CCR4-NOT complex mediates deadenylation and degradation of stem cell mRNAs and promotes planarian stem cell differentiation. *PLOS Genet.* **9**, e1004003 (2013). [doi:10.1371/journal.pgen.1004003](https://doi.org/10.1371/journal.pgen.1004003) [Medline](#)
56. H. Brandl, H. Moon, M. Vila-Farré, S. Y. Liu, I. Henry, J. C. Rink, PlanMine—a mineable resource of planarian biology and biodiversity. *Nucleic Acids Res.* **44**, D764–D773 (2016). [doi:10.1093/nar/gkv1148](https://doi.org/10.1093/nar/gkv1148) [Medline](#)
57. A. Dobin, C. A. Davis, F. Schlesinger, J. Drenkow, C. Zaleski, S. Jha, P. Batut, M. Chaisson, T. R. Gingeras, STAR: Ultrafast universal RNA-seq aligner. *Bioinformatics* **29**, 15–21 (2013). [doi:10.1093/bioinformatics/bts635](https://doi.org/10.1093/bioinformatics/bts635) [Medline](#)
58. V. D. Blondel, J.-L. Guillaume, R. Lambiotte, E. Lefebvre, Fast unfolding of communities in large networks. *J. Stat. Mech. Theory Exp.* **2008**, P10008 (2008). [doi:10.1088/1742-5468/2008/10/P10008](https://doi.org/10.1088/1742-5468/2008/10/P10008)
59. A. Cardona, J. Fernández, J. Solana, R. Romero, An in situ hybridization protocol for planarian embryos: Monitoring myosin heavy chain gene expression. *Dev. Genes Evol.* **215**, 482–488 (2005). [doi:10.1007/s00427-005-0003-1](https://doi.org/10.1007/s00427-005-0003-1) [Medline](#)
60. F. A. Wolf, P. Angerer, F. J. Theis, SCANPY: Large-scale single-cell gene expression data analysis. *Genome Biol.* **19**, 15 (2018). [doi:10.1186/s13059-017-1382-0](https://doi.org/10.1186/s13059-017-1382-0) [Medline](#)
61. S. M. C. Robb, E. Ross, A. Sánchez Alvarado, SmedGD, The *Schmidtea mediterranea* genome database. *Nucleic Acids Res.* **36**, D599–D606 (2008). [doi:10.1093/nar/gkm684](https://doi.org/10.1093/nar/gkm684) [Medline](#)
62. T. Kohonen, J. Hynninen, J. Kangas, J. Laaksonen, Som pak: The self-organizing map program package. *Rep A31, Helsinki Univ Technol Lab Comput Inf Sci* (1996).
63. D. van Dijk *et al.*, MAGIC: A diffusion-based imputation method reveals gene-gene interactions in single-cell RNA-sequencing data. *bioRxiv* (2017). [doi:10.1101/111591](https://doi.org/10.1101/111591)
64. A. McDavid, G. Finak, P. K. Chattopadhyay, M. Dominguez, L. Lamoreaux, S. S. Ma, M. Roederer, R. Gottardo, Data exploration, quality control and testing in single-cell qPCR-based gene expression experiments. *Bioinformatics* **29**, 461–467 (2013). [doi:10.1093/bioinformatics/bts714](https://doi.org/10.1093/bioinformatics/bts714) [Medline](#)
65. J. J. Collins 3rd, X. Hou, E. V. Romanova, B. G. Lambrus, C. M. Miller, A. Saberi, J. V. Sweedler, P. A. Newmark, Genome-wide analyses reveal a role for peptide hormones in planarian germline development. *PLOS Biol.* **8**, e1000509 (2010). [doi:10.1371/journal.pbio.1000509](https://doi.org/10.1371/journal.pbio.1000509) [Medline](#)
66. T. M. J. Fruchterman, E. M. Reingold, Graph drawing by force-directed placement. *Softw. Pract. Exper.* **21**, 1129–1164 (1991). [doi:10.1002/spe.4380211102](https://doi.org/10.1002/spe.4380211102)
67. A. H. Rizvi, P. G. Camara, E. K. Kandror, T. J. Roberts, I. Schieren, T. Maniatis, R. Rabadan, Single-cell topological RNA-seq analysis reveals insights into cellular differentiation and development. *Nat. Biotechnol.* **35**, 551–560 (2017). [doi:10.1038/nbt.3854](https://doi.org/10.1038/nbt.3854) [Medline](#)
68. P. Qiu, E. F. Simonds, S. C. Bendall, K. D. Gibbs Jr., R. V. Bruggner, M. D. Linderman, K. Sachs, G. P. Nolan, S. K. Plevritis, Extracting a cellular hierarchy from high-dimensional cytometry data with SPADE. *Nat. Biotechnol.* **29**, 886–891 (2011). [doi:10.1038/nbt.1991](https://doi.org/10.1038/nbt.1991) [Medline](#)
69. C. Trapnell, D. Cacchiarelli, J. Grimsby, P. Pokharel, S. Li, M. Morse, N. J. Lennon, K. J. Livak, T. S. Mikkelsen, J. L. Rinn, The dynamics and regulators of cell fate decisions are revealed by pseudotemporal ordering of single cells. *Nat. Biotechnol.* **32**, 381–386 (2014). [doi:10.1038/nbt.2859](https://doi.org/10.1038/nbt.2859) [Medline](#)
70. G. Gieco, E. Marco, S. P. Garcia, L. Trippa, G.-C. Yuan, Robust lineage reconstruction from high-dimensional single-cell data. *Nucleic Acids Res.* **44**, e122–e122 (2016). [doi:10.1093/nar/gkw452](https://doi.org/10.1093/nar/gkw452) [Medline](#)
71. Z. Ji, H. Ji, TSCAN: Pseudo-time reconstruction and evaluation in single-cell RNA-seq analysis. *Nucleic Acids Res.* **44**, e117–e117 (2016). [doi:10.1093/nar/gkw430](https://doi.org/10.1093/nar/gkw430) [Medline](#)
72. J. Chen, A. Schlitzer, S. Chakarov, F. Ginhoux, M. Poidinger, Mpath maps multi-branching single-cell trajectories revealing progenitor cell progression during development. *Nat. Commun.* **7**, 11988 (2016). [doi:10.1038/ncomms11988](https://doi.org/10.1038/ncomms11988) [Medline](#)
73. X. Qiu, A. Hill, J. Packer, D. Lin, Y.-A. Ma, C. Trapnell, Single-cell mRNA quantification and differential analysis with Census. *Nat. Methods* **14**, 309–315 (2017). [doi:10.1038/nmeth.4150](https://doi.org/10.1038/nmeth.4150) [Medline](#)
74. K. A. Janes, Single-cell states versus single-cell atlases - two classes of heterogeneity that differ in meaning and method. *Curr. Opin. Biotechnol.* **39**, 120–125 (2016). [doi:10.1016/j.copbio.2016.03.015](https://doi.org/10.1016/j.copbio.2016.03.015) [Medline](#)

## ACKNOWLEDGMENTS

We thank J. Alles and A. Boltengagen for help with single-cell sequencing and members of the Rajewsky lab for many discussions. We thank S. Linnarsson and G.e La Manno for helping to run velocity. We also thank N. Friedman and A. García-Pérez for useful comments. The work in this project was funded by the German center for Cardiovascular Research (DZHK BER 1.2 VD), the DFG grant RA 838/5-1, the BMBF (grant #01ZX1711A), and the Helmholtz Association (Incubator grant sparse2big, grant #ZT-I-0007). FAW acknowledges the support of the Helmholtz Postdoc Program, Initiative and Networking Fund of the Helmholtz Association. Author contributions: JS, MP, CK and NR designed the project. JS, CK, and NR designed all experiments. SA, JS, and CK performed all experiments. MP performed and coordinated computational analyses. FAW performed the PAGA analysis with the supervision of FJT. AM performed velocity analyses. PG developed the Shiny app and performed image analysis. BO developed the visualization of gene expression along the lineage tree. All authors discussed and interpreted the data. MP, JS and NR wrote the manuscript with input from all other authors. Competing interests: authors declare no competing interests. Data and materials availability: The sequencing data generated is available in GEO under the accession GSE103633. The single cell data generated can be interactively accessed at <https://shiny.mdc-berlin.de/psca>. Manuals to run and reproduce velocity and PAGA are available

on Github [https://github.com/rajewsky-lab/planarian\\_lineages](https://github.com/rajewsky-lab/planarian_lineages).

#### **SUPPLEMENTARY MATERIALS**

[www.sciencemag.org/cgi/content/full/science.aaq1723/DC1](http://www.sciencemag.org/cgi/content/full/science.aaq1723/DC1)

Materials and Methods

Supplementary Text

Figs. S1 to S22

Tables S1 to S10

References (54–74)

9 October 2017; resubmitted 14 February 2018

Accepted 12 April 2018

Published online 19 April 2018

10.1126/science.aaq1723



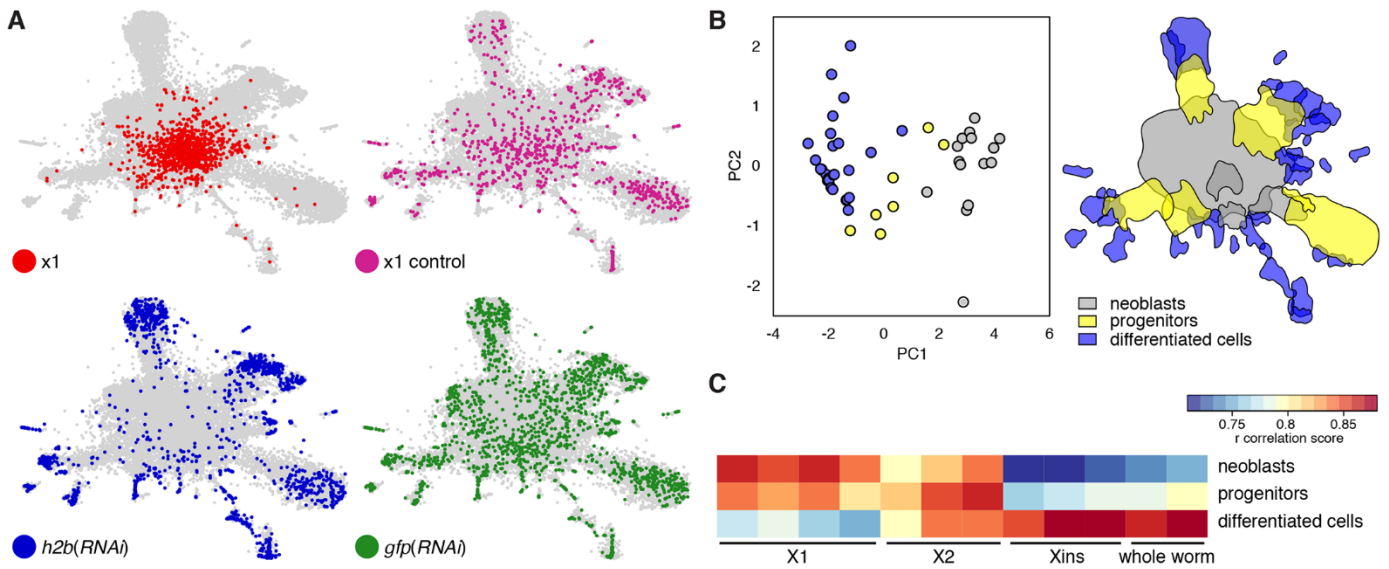


**Fig. 2. Neoblast ablation and enrichment experiments show stem and progenitor clusters.** **A.** tSNE plots showing the distribution of the cells of an X1 FACS sorted sample (red) and its whole cell population control (x1 control, magenta), and a *h2b(RNAi)* sample with its negative control (*gfp(RNAi)*, green). X1 cells are enriched in the center of the plot while *h2b(RNAi)* cells are enriched in the periphery. **B.** PCA analysis considering the expression level of neoblast marker genes and the log odds ratio of the amount of cells per cluster from *h2b(RNAi)* and X1 experiments compared to wt and control samples separates neoblasts (grey), progenitor clusters (yellow) and differentiated cell clusters (blue). The location of these clusters is shown on the tSNE plot on the right. **C.** Gene expression correlation between bulk RNA-seq data from FACS sorted X1, X2, Xins populations and whole worms and the pooled clusters as defined in **B**. Neoblasts show a stronger correlation with X1, progenitors with X2, and differentiated cells with Xins and whole worms.

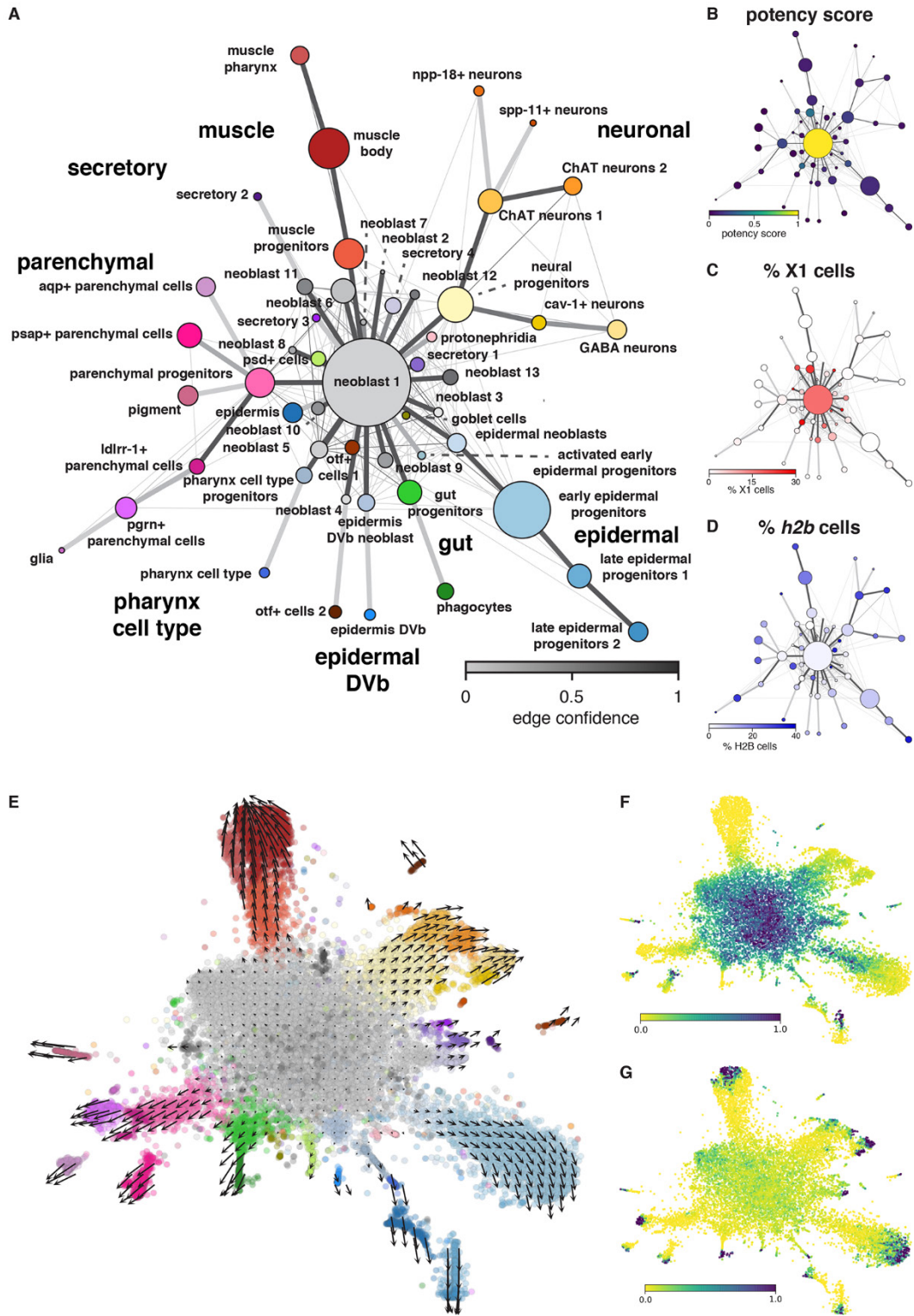


**Fig. 3. Lineage tree reconstruction by PAGA and velocyto.** **A.** Abstracted graph showing all the possible edges with a probability higher than  $10e-6$  connecting two clusters and their confidence. Each node corresponds to each of the clusters identified using Seurat. The size of nodes is proportional to the amount of cells in the cluster. The most probable path connecting the clusters is plotted on top with thicker edges. **B.** Lineage tree colored according to potency score, which ranges from blue (0) to yellow (1). **C, D.** Lineage trees colored according to the % of X1 (**C**) or *h2b(RNAi)* resistant (**D**) cells in each cluster. X1 cells are most abundant in the neoblast 1 cluster whereas *h2b(RNAi)* resistant cells are mostly located in the leaves of the tree. **E.** Velocyto force field showing the average differentiation trajectories (velocity) for cells located in different parts of the tSNE plot. **F, G.** Root (**F**) and terminal end-points (**G**) obtained after modeling the transition probabilities derived from the RNA velocity using a Markov Process. The color scale represents the density of the end points of the Markov Process and ranges from yellow (low) to blue (high).

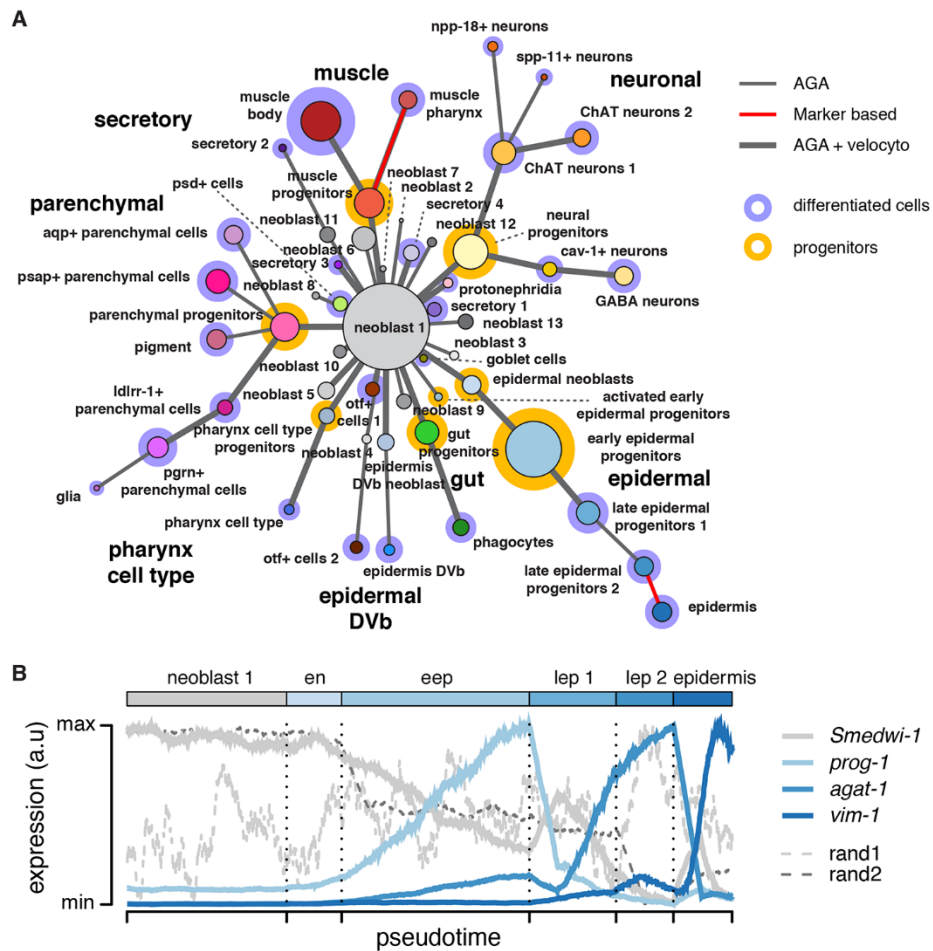


**Fig. 4. Consolidated lineage tree of planarian stem cell differentiation into all major types.** **A.** Consolidated lineage tree including 4 independent sources of evidence. The topology of the tree is shown according to PAGA, marker-based connections are shown with red edges. Velocityto supported connections are shown with thick edges. Progenitor and differentiated cell clusters according to neoblasts ablation and enrichment experiments are shown with yellow and blue halos, respectively. **B.** Gene expression changes of marker genes for the individual stages during epidermal differentiation (in pseudotime). Relative expression of marker genes from neoblast (*Smedwi-1*), early (*prog-1*) and late (*agat-1*) progenitors as well as from the epidermis (*vim-1*). A maximum of 1000 cells from neoblast 1, epidermal neoblasts (en), early epidermal progenitors (eep), late epidermal progenitors 1 (lep 1) and 2 (lep 2) and epidermis were sampled. Grey thin dashed lines show the expression of *Smedwi-1* after randomly permuting cells (rand 1) or after randomly sorting cells within each cluster (rand 2).

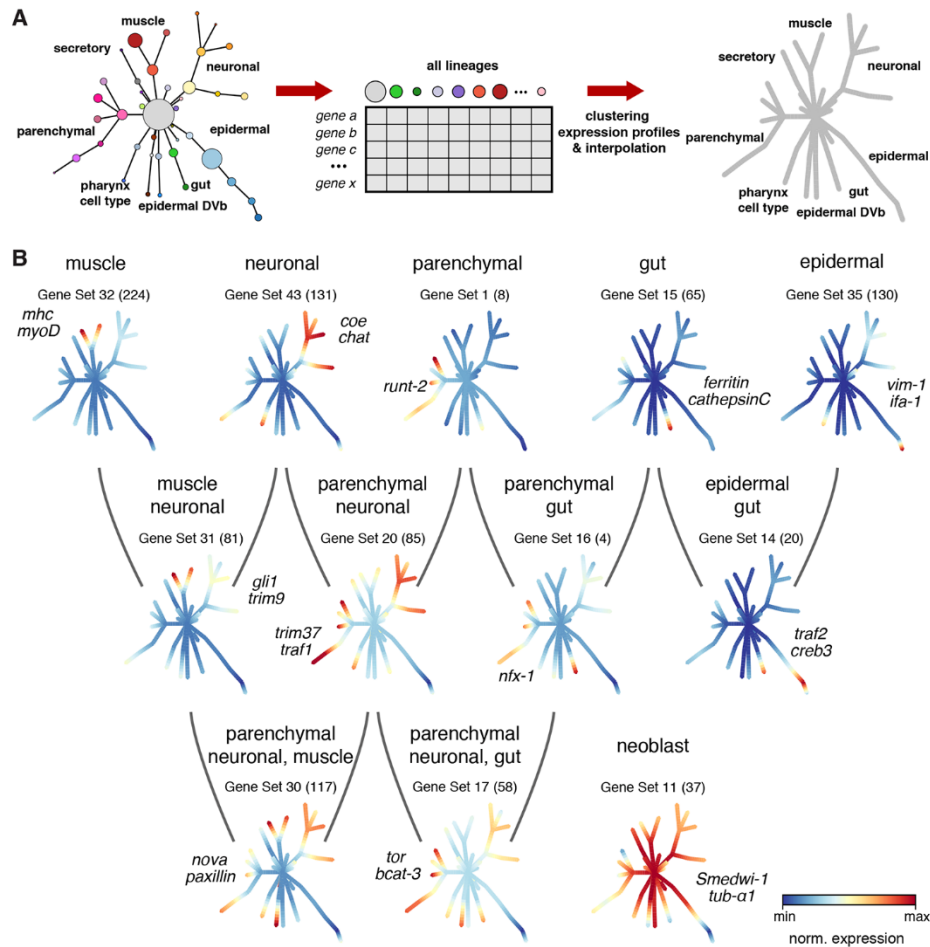


**Fig. 5. Identification of gene sets regulated and coregulated in cell differentiation.** **A.** Schematic workflow of the analysis performed to identify gene sets involved in lineage decisions. Pseudotemporal ordering of the cells from all lineages and clustering of variable genes using SOMs allowed the identification of 48 gene sets. **B.** Graphical representation of gene expression changes during cell differentiation of 12 gene sets. For each gene set, the normalized expression of the genes is shown on the edges of the tree and ranges from blue (low expression) to red (high expression). Next to each tree, representative genes from each gene set are highlighted.

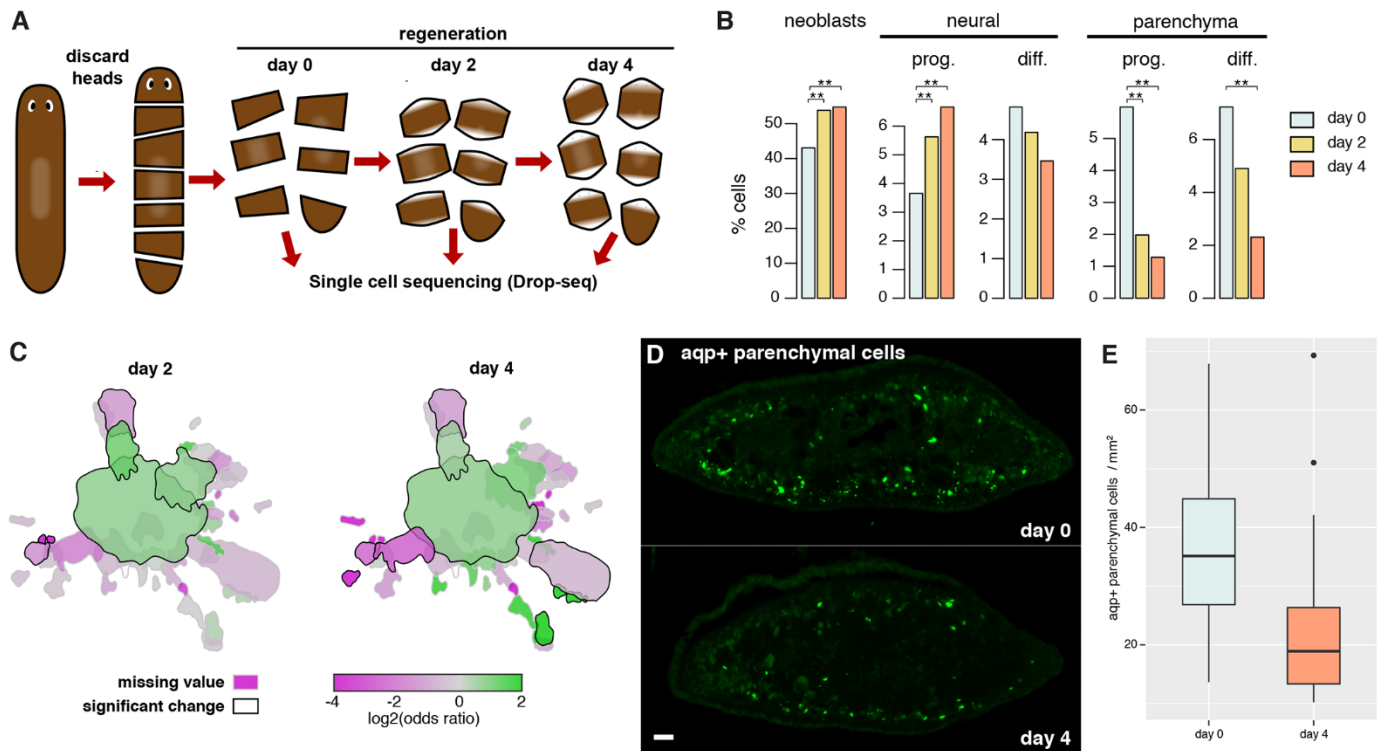


**Fig. 6. Molecular profiling of regeneration by single-cell transcriptomics.** **A.** Experimental workflow: planarians were cut into small pieces, head pieces were discarded and the remaining pieces were processed for single-cell RNA sequencing 0, 2 and 4 days after cut. **B.** Quantification of neoblasts, neural progenitors and differentiated clusters and parenchymal progenitors and differentiated clusters. Significant differences calculated using a fisher test with an adjusted p-value < 0.001 are marked with \*\*. **C.** Cluster outlines colored according to the log<sub>2</sub> (odds ratio) of changes in regeneration at day 2 (left) and day 4 (right) vs day 0, showing enriched clusters in green colors and depleted clusters in magenta colors. Significant changes are indicated by black solid outlines. **D, E.** In situ hybridization on sections (D) and quantification (E) of aqp+ parenchymal cells in regenerating planarians after 0 and 4 days of regeneration. Mann Whitney U-test p-value < 10e-7. Scale bar: 100 μm.

## Cell type atlas and lineage tree of a whole complex animal by single-cell transcriptomics

Mireya Plass, Jordi Solana, F. Alexander Wolf, Salah Ayoub, Aristotelis Misios, Petar Glazar, Benedikt Obermayer, Fabian J. Theis, Christine Kocks and Nikolaus Rajewsky

published online April 19, 2018

ARTICLE TOOLS	<a href="http://science.sciencemag.org/content/early/2018/04/18/science.aaq1723">http://science.sciencemag.org/content/early/2018/04/18/science.aaq1723</a>
SUPPLEMENTARY MATERIALS	<a href="http://science.sciencemag.org/content/suppl/2018/04/18/science.aaq1723.DC1">http://science.sciencemag.org/content/suppl/2018/04/18/science.aaq1723.DC1</a>
RELATED CONTENT	<a href="http://science.sciencemag.org/content/sci/360/6391/eaq1736.full">http://science.sciencemag.org/content/sci/360/6391/eaq1736.full</a>
REFERENCES	This article cites 71 articles, 13 of which you can access for free <a href="http://science.sciencemag.org/content/early/2018/04/18/science.aaq1723#BIBL">http://science.sciencemag.org/content/early/2018/04/18/science.aaq1723#BIBL</a>
PERMISSIONS	<a href="http://www.sciencemag.org/help/reprints-and-permissions">http://www.sciencemag.org/help/reprints-and-permissions</a>

Use of this article is subject to the [Terms of Service](#)